THE ASTROPHYSICAL JOURNAL, 455:603–613, 1995 December 20

THE IRON L/K EMISSION-LINE RATIO IN PHOTOIONIZED GASES

T. R. KALLMAN
Laboratory for High Energy Astrophysics, NASA/Goddard Space Flight Center, Greenbelt, MD 20771
Received 1995 April 17; accepted 1995 June 30

ABSTRACT

We present models for the emission spectra of photoionized gases in the intermediate energy (0.5–10 keV) X-ray region. We discuss the general properties of iron K and L shell emission features—line strengths and recombination continuum emission—and compare the strengths of these features with iron K shell emission and with the spectral features produced by other elements in the same energy range. We show that there is effectively an upper bound to the L/K ratio, and we compare this with the strengths of the features observed from medium-resolution spectra of X-ray binaries and active galaxies.

Subject headings: atomic processes — binaries: close — galaxies: active

1. INTRODUCTION

Iron lines have a unique importance in aiding understanding of the spectra of many X-ray sources. This is particularly true for X-ray binaries and other objects in which it is likely that photoionization dominates the ionization processes. The line strengths depend on both the conditions in the emitting gas and on the broadband properties of the ionizing continuum. Furthermore, the energies of the iron K lines and the ratio of the L lines of iron and the K lines of medium-Z elements to the iron K lines are probes of the ionization state in the gas near the compact object. The continuing advances in X-ray detector technology have resulted in many new observations of the iron lines from X-ray binaries, and this trend is likely to continue over the next 10 years or so. It is therefore useful to study the systematic behavior of the iron lines in photoionized plasmas as a function of the various free parameters which affect their emission efficiency. This paper is the first of a series on this subject.

This paper will discuss the formation of iron line features in photoionized gases. The emphasis will be on the intrinsic efficiency of the line formation and on the energies of the emitted lines. These will be explored first in the case of idealized models for the line-emitting region and then will be discussed briefly in the context of more realistic models for X-ray binary–(XRB) emitting regions. Later papers will present more detailed models for the iron L shell spectra and will fit these models to data from XRBs.

2. PHOTOIONIZATION MODELS FOR IRON LINE EMISSION

The relative importance of the various processes affecting iron line emission can be illustrated by considering the line emission spectra from an idealized model for the emission-line region in an XRB. The model that we consider consists of a slab of gas with constant density that is heated by ionizing radiation from a compact object with prescribed spectrum and flux. The line emission arises as a consequence of the absorption and reprocessing by this gas. The physical processes affecting the heating, ionization, and excitation of the gas are all assumed to be in a steady state, and the elemental abundances are solar (Withbroe 1971). The results of such photoionization models depend on the shape of the ionizing continuum, on the column density of the slab, and on the ratio of the continuum flux at the illuminated face of the slab to the gas density, the ionization parameter. We adopt the following definition for the ionization parameter: $\xi = 4\pi F/n$ (Tarter, Tucker, & Salpeter 1969) and assume the gas density n is fixed. Alternative definitions for ionization parameter may be used when the gas pressure is fixed, but we will not consider them in this paper. We define F as the radiation energy flux in ergs cm^{-2} s^{-1} integrated between the energies of 1 and 1000 ryd. At large ionization parameter the gas is more ionized and hotter, and conversely the degree of ionization of the various elements and the temperature are lower at small ionization parameter (e.g., Kallman & McCray 1982).

In the following sections we present analytic estimates and numerical calculations of the emissivities of iron lines in the X-ray spectral range, 0.5–10 keV. The numerical results have been calculated using the code described by Kallman & Krolik (1993) and by Kallman & McCray (1982). The calculations assume a stationary balance between heating and cooling and between various processes affecting ionization and recombination and are described in more detail in the Appendix.

2.1. *K Lines*

Iron is unique among the most abundant elements in the relatively high efficiency for inner shell fluorescence. This is due to the abundance of iron and to the fact that the transition rate for decay of the multiply excited level produced by inner shell ionization scales more rapidly with the nuclear charge than does the rate for the competing process, Auger ionization (e.g., Bambynek et al. 1972). The fluorescence yield ω is described as the probability that a K line photon is emitted following the removal of a K shell electron by photoionization, and ranges from 0.34 in Fe I to 0.49 in Fe XXII (Bambynek et al. 1972; Jacobs & Rozsnyai 1986). In Fe XXIII the yield drops to $\omega = 0.11$, and in Fe XXIV it is ~ 0.75 (Krolik & Kallman 1987). The energy $\epsilon_{K\alpha}$ of the Kα photon is $\simeq 6.4$ keV in Fe I through Fe XXVII, increasing at higher ionization stages up to nearly 7 keV in Fe XXVI (Makishima 1986). The rate of line emission also depends on the photoionization cross section and its behavior as a function of ionization state. The energy of the edge moves from 8.49 keV to 8.76 keV, and the threshold cross section moves from 2.19×10^{-20} cm^2 to 2.02×10^{-20} cm^2 between Fe XXIII and Fe XXV.

For Fe XXVI, recombination from Fe XXVII is likely to be the dominant emission process in a photoionized gas, since there is no inner shell fluorescence in this ion and the temperature in a

photoionized plasma is likely to be too low to allow efficient collisional excitation. The relevant recombination rate can be derived from cascade matrix calculations familiar from the study of nebular hydrogen emission lines (e.g., Osterbrock 1974). In a steady state the recombination into Fe XXVI is balanced by photoionization, so the line emission rate per Fe XXVI ion will be proportional to the photoionization rate coefficient. The constant of proportionality is equivalent to a fluorescence yield and is in the range $\omega_{\text{Fe XXVI}} \simeq 0.3$–$0.7$ depending on temperature and assumptions about the nature of the recombination cascade process. Iron emission features can also be formed by scattering of line photons into the observer's line of sight, as pointed out by Band et al. (1990). The efficiency for this process depends formally on the oscillator strengths for the various lines involved. Since sum rules guarantee that the summed line oscillator strengths will be comparable in magnitude to those for the continuum, i.e., the photoionization cross section, it follows that this process will have intrinsic efficiency comparable to K shell fluorescence. Both processes will have lower macroscopic efficiency at large column densities when the emission or scattering region is shielded from the incident continuum. The difference between the two lies in the fact that scattering saturates at lower columns owing to the smaller bandwidth, and hence greater cross section, for line absorption as opposed to continuum processes. Another important difference lies in the fact that scattering of K lines can only occur for ions with unfilled L shells, i.e., Fe XVIII–Fe XXVI. For ions Fe XVIII–Fe XXIV, scattering works with comparable efficiency for both L lines and K lines.

A convenient way of characterizing the efficiency of reprocessing continuum photons into iron lines is in terms of the equivalent width. A simple estimate of this quantity for fluorescence from an optically thin slab is

$$\text{EW} \simeq \epsilon_{\text{line}} \frac{L_\epsilon|_{\epsilon=\epsilon_{\text{th}}}}{L_\epsilon|_{\epsilon=\epsilon_{\text{line}}}} \sigma_{\text{th}}\, \omega x y N\,, \qquad (1)$$

where EW is the line equivalent width, ϵ_{line} is the line energy, $L_\epsilon|_{\epsilon=\epsilon_{\text{th}}}$ is the ionizing specific luminosity evaluated at the threshold energy of the emitting ion, $L_\epsilon|_{\epsilon=\epsilon_{\text{line}}}$ is the ionizing specific luminosity at the line energy, σ_{th} is the K shell photoionization cross section at the threshold energy, ω is the fluorescence yield, x is the ionization fraction of the emitting ion, y is the elemental abundance of iron, and N is the total column of the reprocessor. If the spectrum is flat between the line and the K edge, $x = 1$, $y = 3 \times 10^{-5}$ and we take the cross section for neutral iron, then the equivalent width will be approximately EW $\simeq 2.3$ keV N_{24}, where N_{24} is the cloud column density in units of 10^{24} cm^{-2}. These assumptions are likely to be valid only when the dominant line production mechanism is inner shell fluorescence. When the dominant line emission mechanism is recombination, the abundance of the emitting ion, x, is likely to depend sensitively on ionization parameter.

At column densities greater than about 10^{24} cm^{-2} the approximate formula (1) breaks down, owing to the effects of absorption and scattering of the continuum photons as they enter the slab and of line photons as they leave. Both these effects cause the reprocessing efficiency to decrease at large columns relative to the estimate of equation (1) (Makishima 1986, and references therein). This decrease will depend on the detailed radiation transfer processes which can, for example, redistribute ionizing photons into or out of the ionizing continuum of the various iron ions. It will also depend on the geometry of the reprocessor and the incident continuum. For example, a slab seen in reflection is likely to present a smaller column to the emitted line photons, since they will traverse a "bleached" region as they escape, than it will to line photons if it is viewed in transmission.

A more accurate estimate of the efficiency of reprocessing is given by the numerical photoionization model results shown in Figure 1*a*. This shows the log of the line luminosity in units of 10^{38} ergs s^{-1} emitted by model slabs (which may be optically thick) as viewed in transmission (*solid lines*) and in reflection (*dashed lines*) as a function of ionization parameters for various column densities $N = 10^{20}$ cm^{-2} to $10^{23.5}$ cm^{-2}. The line luminosity corresponds to what an observer would see from an ensemble of such slabs arranged into a spherical shell completely surrounding the source of ionizing continuum. The two sets of curves are overlapping, or nearly so, whenever the clouds are optically thin. This occurs at high ionization parameter and low column density. The continuum is assumed to be a power-law spectrum with energy index -1 and a total ionizing luminosity of 10^{38} ergs s^{-1}. Since any given model can emit a complex of lines from several ionization states, we define the line energy ϵ_{line} to be the luminosity-weighted average of the various components. The values of this quantity are shown in Figure 2*a*. The Appendix describes the numerical procedure used in these calculations.

The range of ionization parameters and column densities for which the clouds are optically thin at the energy of the iron K lines is approximately log $(\xi) \geq 2.5$ for a column of $10^{23.5}$ cm^{-2} and the entire range spanned by the models for smaller column densities. At $N = 10^{25}$ cm^{-2} the clouds are optically thick at all values of ionization parameter; we do not attempt to treat such high columns owing to the likely importance of Compton scattering on the escaping spectrum. Our numerical technique is better suited to transfer problems dominated by pure absorption rather than scattering. Within the optically thin range, the estimates of equation (1) are crudely consistent with the numerical results. The line luminosity is proportional to the cloud column density, and the maximum attainable line equivalent width is approximately 95 eV at a column of 10^{23} cm^{-2} when emission from both faces of the slabs are included.

The line equivalent width decreases with increasing ionization parameter at large ionization parameter owing to the depletion of ions with any bound electrons. In the limit of fully stripped iron we expect the emitted luminosity to scale proportional to ξ^{-1}, in accord with the numerical results. Also apparent in Figure 1*a* is a local maximum in the emitted luminosity near log $\xi = 3$, which is due to the enhanced fluorescence efficiency for Fe XXIV. The monotonic decrease between log $\xi = 2$ and log $\xi = 3$ is due to the decrease in fluorescence efficiency from Fe XXIII and to the decreased K shell cross section and the increased threshold energy from Fe XVIII–Fe XXIII.

Departures from the optically thin approximation are also apparent from the asymmetry between the luminosities of the reflected and transmitted line components. This is most obvious at low values of ionization parameter (log $\xi \leq 2$) for a cloud column density of $10^{23.5}$ cm^{-2}, where the ratio between the two components is approximately 1.5:1. At large ionization parameters for this choice of column the cloud is sufficiently highly ionized that absorption of the line photons as they escape is unimportant. However, effects of absorption for log $\xi \geq 2.5$ and column density $10^{23.5}$ cm^{-2} can be discerned

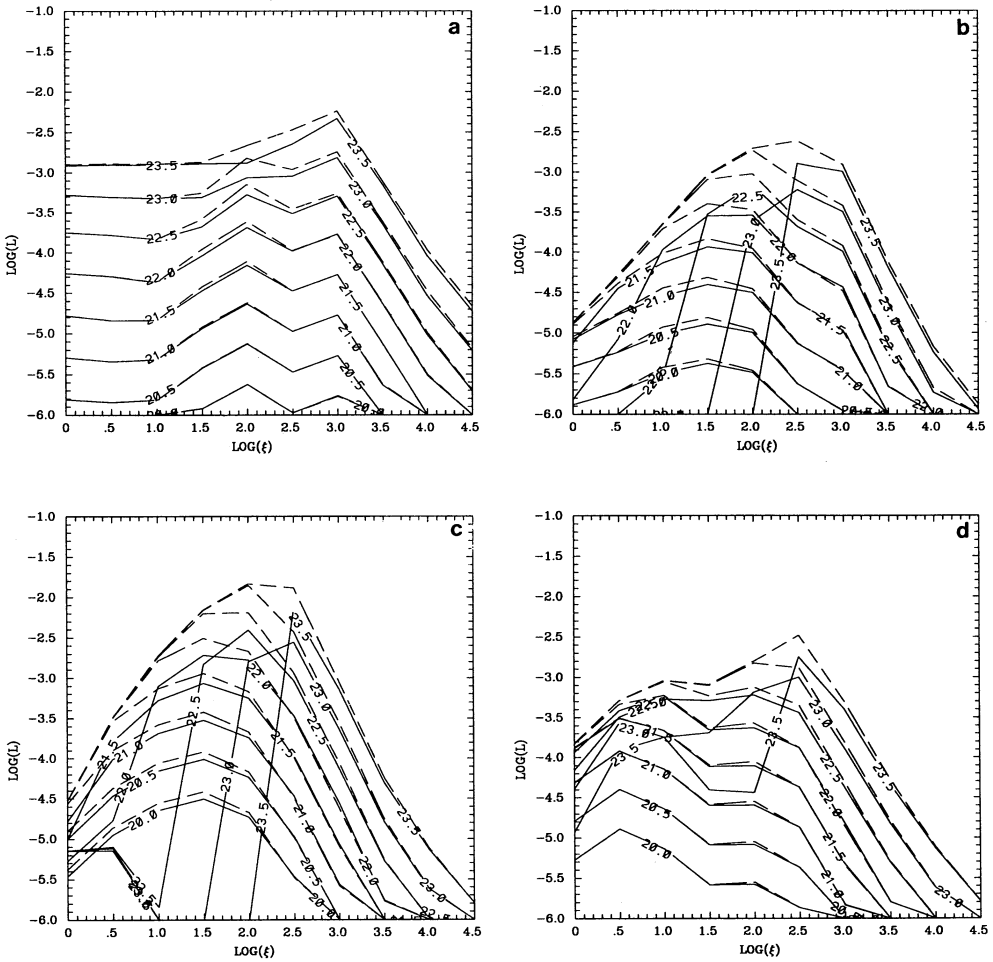

FIG. 1.—Luminosities of various emission lines emitted by constant density slabs of varying column density. Lines reflected from the illuminated face of the slab are shown as the dashed curves, and lines emitted from the unilluminated face of the slabs are shown as solid curves. Curves are labeled by the log of the slab column density (reflected curves are not labeled for clarity). The luminosity is fractional relative to the total ionizing luminosity, and the continuum is assumed to be a power law with index -1. The various panels are for various lines: (*a*) iron K lines; (*b*) iron L lines; (*c*) oxygen K lines; (*d*) silicon K lines.

from the difference between the energies of the reflected and transmitted lines. This is because the line photons emitted by more highly ionized material near the illuminated face of the cloud escape preferentially from that face, while the photons escaping the unilluminated face of the cloud are more likely to be emitted far from the illuminated face. Absorption within the cloud of the incident ionizing continuum photons causes the material farther from the illuminated face to be less highly ionized, and hence to emit a lower energy line, than material close to the illuminated face.

2.2. *L Lines*

A consequence of the screening of nuclear charge by the K electrons is that fluorescent yields for the emission of L lines are never greater than 10^{-2} for near-neutral iron ions (e.g., Bambynek et al. 1972; Jacobs & Rosznyai 1986). Therefore efficient L line emission can come only from ions Fe XVI and higher. Fe XVI can emit via L shell fluorescence owing to the absence of nonradiative decay channels of the excited ion left after the L shell ionization of Fe XV. Fe XVII–XXVI can emit following collisional excitation or recombination.

Estimates of L line intensities are complicated by the many possible line transitions and by the variety of physical processes which can lead to line emission (e.g., Liedahl et al. 1990). Also, the greater number of potentially observable lines and the larger spectral band they cover makes simple estimates necessarily much more crude. For either recombination or collisional excitation, the line equivalent width can be written in terms of an effective "fluorescence yield" using equation (1), where the yield is defined in the same sense as it is for the recombination emission of K lines from Fe XXV and XXVI. That is, the yield is the fraction of recombinations into an ion which result in L line emission. Collisional excitation may also be included in this description if the yield includes the ratio of the rates of excitation to photoionization.

Rather than present analytic estimates for these rates, we show in Figure 1*b* the results of numerical calculations of the L line intensities from the same model slabs described in the previous subsection and in the Appendix. We consider these results to be accurate to within a factor of 2, sufficient for comparison with medium-resolution ($\Delta\epsilon/\epsilon \simeq 10$) observations such as those obtained with the solid state detectors on the *Einstein* (*HEAO-2*), *BBXRT*, and *ASCA* spacecraft.

Figures 1*c* and 1*d* show the luminosities from the K lines of oxygen and silicon, respectively, since medium-resolution detectors can distinguish between these lines and the L shell of

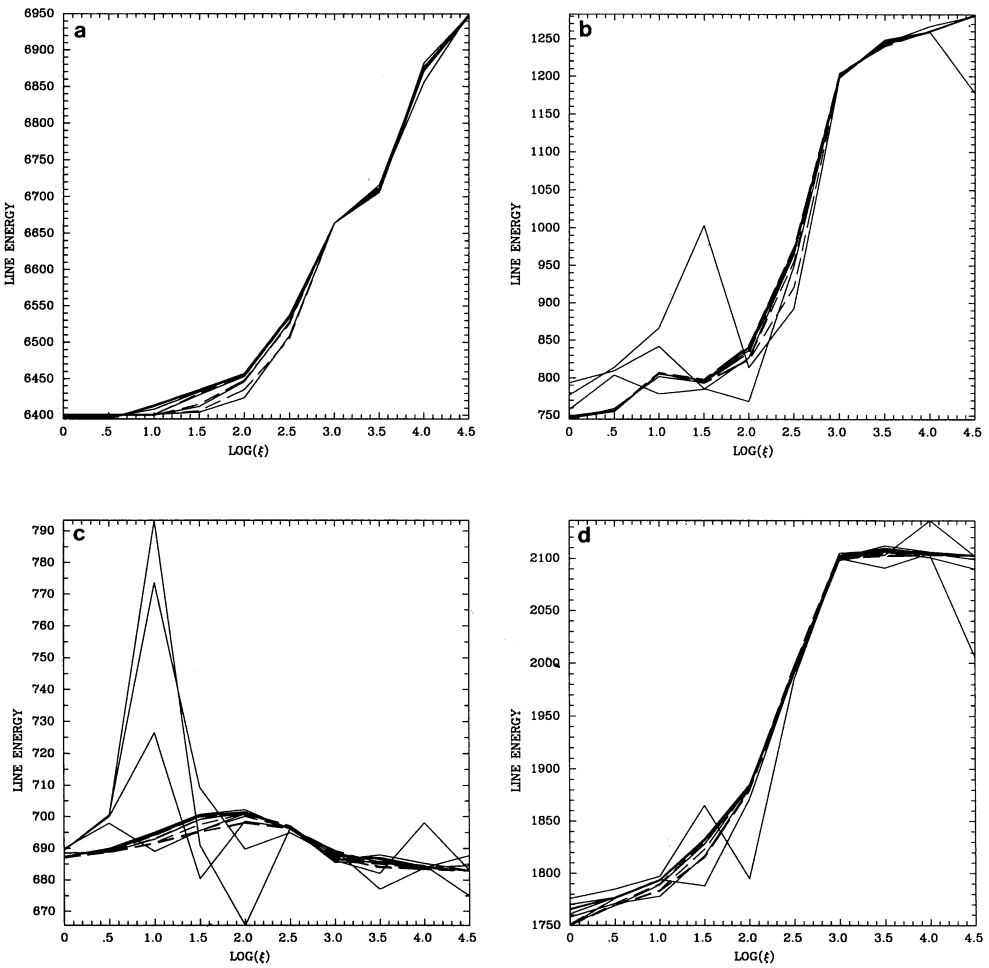

FIG. 2.—Mean energies (eV) of various emission lines emitted by constant density slabs of varying column density. Lines reflected from the illuminated face of the slab are shown as the dashed curves, and lines emitted from the unilluminated face of the slabs are shown as solid curves. The continuum is assumed to be a power law with index −1. The various panels are for various lines: (*a*) iron K lines; (*b*) iron L lines; (*c*) oxygen K lines; (*d*) silicon K lines.

iron. These panels show that the contributions from the various lines are all comparable, although peak luminosities occur at higher ionization parameter for the silicon lines (log $\xi \simeq 2.5$), and at lower ionization parameter for the oxygen lines (log $\xi \simeq 2$), while the iron L lines' peak occurs at intermediate ionization parameter.

The scaling behavior of L lines is qualitatively similar to that of the K lines: The emitted luminosities are approximately proportional to cloud column density at large ξ, when the optically thin approximation obtains. The luminosities also decrease proportional to ξ in this region, owing to the depletion of ions with L shell electrons. For $\xi \sim 2.5$ the luminosity passes through a maximum, with the decrease at lower ξ due to the fact that ions with M shell electrons predominate. In this range of ionization parameter, the optically thin assumption is invalid, resulting in luminosities which do not scale with column density, and in large asymmetries between the reflected and transmitted components.

Of particular interest to current observations of XRBs is the ratio of the L line luminosities to those of the K lines. This is because, even if the two sets of lines are emitted from two (or more) separate regions with differing conditions, the total L/K ratio cannot lie outside the range of ratios spanned by the various regions. Figure 1 shows that there is no obvious lower limit on the L/K ratio, but that the upper limit for high column density clouds (near $\xi \simeq 3$ for the $10^{23.5}$ cm^{-2} slab seen in reflection) is approximately 1.6. This maximum L/K ratio value may be regarded as uncertain to within 50%, say, owing to the coarseness of the model grid employed here and to other uncertainties in the models themselves including the uncertainties in the atomic rate data employed for the L line emission calculation. Note also that under the conditions needed for this maximum L/K ratio, the efficiency of making these lines is high but is not the maximum value found in the model grid. The K line equivalent width is 150 eV under these conditions. The ratio of the equivalent widths of the L and K lines is also smaller than the ratios of the luminosities by approximately a factor 1.9 because of the lower continuum flux in the vicinity of the K line for our choice of ionizing spectrum.

Another way of visualizing the L/K ratio is shown in Figure 3, which shows the ratio of reflected line luminosities plotted against ionization parameter for various column densities. This shows that the ratio can be as large as $\simeq 80$, near log $\xi = 1$ for the lowest column densities we consider. This is because the L line production efficiency has a local maximum when the ions Fe XV–XVII are abundant, due in part to inner shell fluorescence following ionization of Fe XV. The K line fluorescence yields, on the other hand, decline monotonically

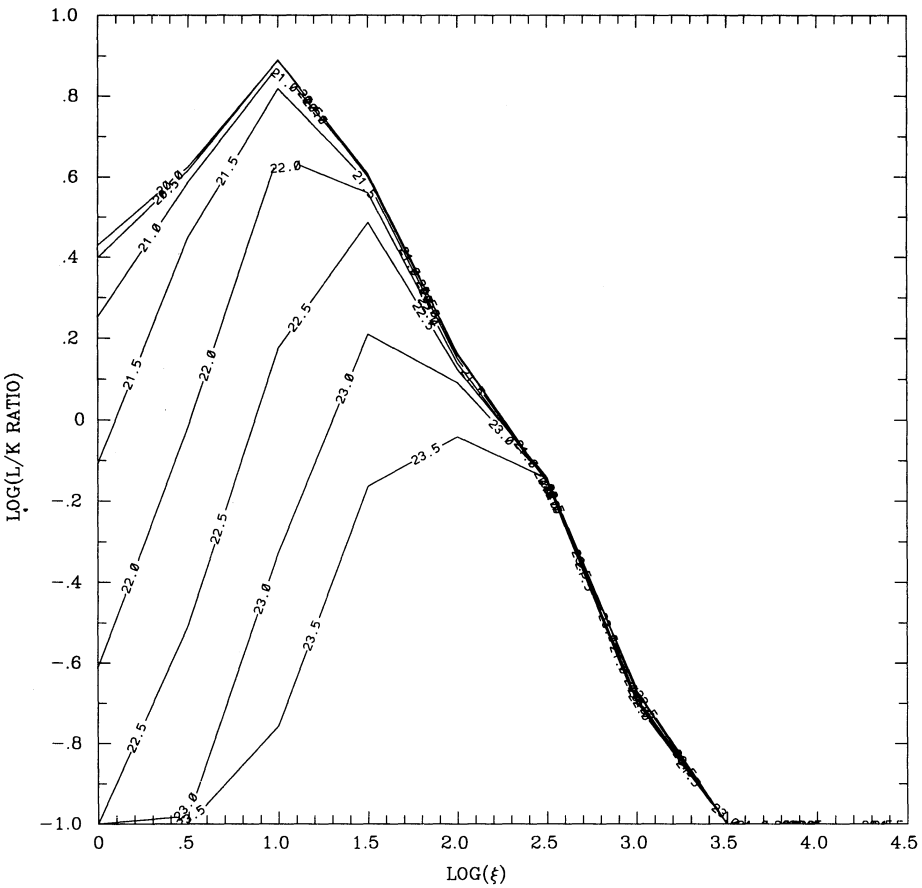

FIG. 3.—Ratio of the luminosities in the iron L and K lines as a function of ionization parameter from the results of model slabs seen in reflection shown in Fig. 1. Curves are labeled by the log of the column density.

with increasing ionization stage. The large L/K ratios occur only for low column clouds because, when the clouds have greater columns and are optically thick to photoelectric absorption at energies near the L shell ionization thresholds, the transition from nearly neutral to highly ionized iron occurs in an increasingly narrow ionization front. Therefore, the large L/K ratios are attainable only at the price of very low line equivalent widths for both the L and K lines. For example, at the peak of the ratio curve shown in Figure 2, the K line equivalent width is 0.02 eV for a column of 10^{20} cm^{-2}. On the other hand, at log $\xi = 2$, and a column of $N = 10^{23.5}$ cm^{-2}, the K line equivalent width is 180 eV. Furthermore, the K line equivalent width scales with proportionality $1/N$, while the L/K ratio scales more slowly, approximately proportional to $N^{1/2}$. Therefore, the lines that we are currently able to detect are most likely to arise in high column gas, where the L/K ratio is likely to be at most of order unity.

In addition to the various emission lines described so far, there exist several other potentially observable features inherent in such models for reprocessed spectra. These include the iron K edges at 7.1–9.3 keV, the various recombination continua, and the absorption at low energies produced by photoionization of electrons bound with energies 0.01–0.6 keV. Although the behavior of these features can be examined in the same way as has been done for the emission lines, comparison of the results with observations depends more sensitively on the instrumental details than do the emission lines, and so we will not present them here.

At this point it is worthwhile to summarize what the idealized slab models tell us about iron line production efficiency and the mean energy of the emitted line. In order to get a high-energy K line, i.e., $\epsilon \geq 6.5$ keV, all that is needed is that the ionization parameter of the reprocessor be greater than log $\xi \simeq 2$. This applies to both low (10^{22} cm^{-2}) and high (10^{24} cm^{-2}) column density clouds, although line energies characteristic of hydrogenic iron can be obtained at high column density only if log $\xi \geq 4$. The converse may also be emphasized: that high ξ material cannot emit a low-energy (6.4 keV) iron line with significant efficiency. This fact has been pointed out in the context of low-mass X-ray binaries by Kallman & White (1988) and in the context of active galaxies by Begelman & deKool (1990). In order to obtain high reprocessing efficiency, as measured either by the line luminosity or the equivalent width, the ionization parameter must be log $\xi \leq 2$, and the column must be $\geq 10^{24}$ cm^{-2}. For any given column density, the greatest efficiency is obtained at log $\xi \leq 2$. To get large L/K ratios the ionization parameter must be near log $\xi \sim 2$–3. The greatest such ratios are obtained at columns less than 10^{21} cm^{-2} but with significantly reduced efficiency.

Figure 2*b* shows the weighted mean energy of the L lines. At

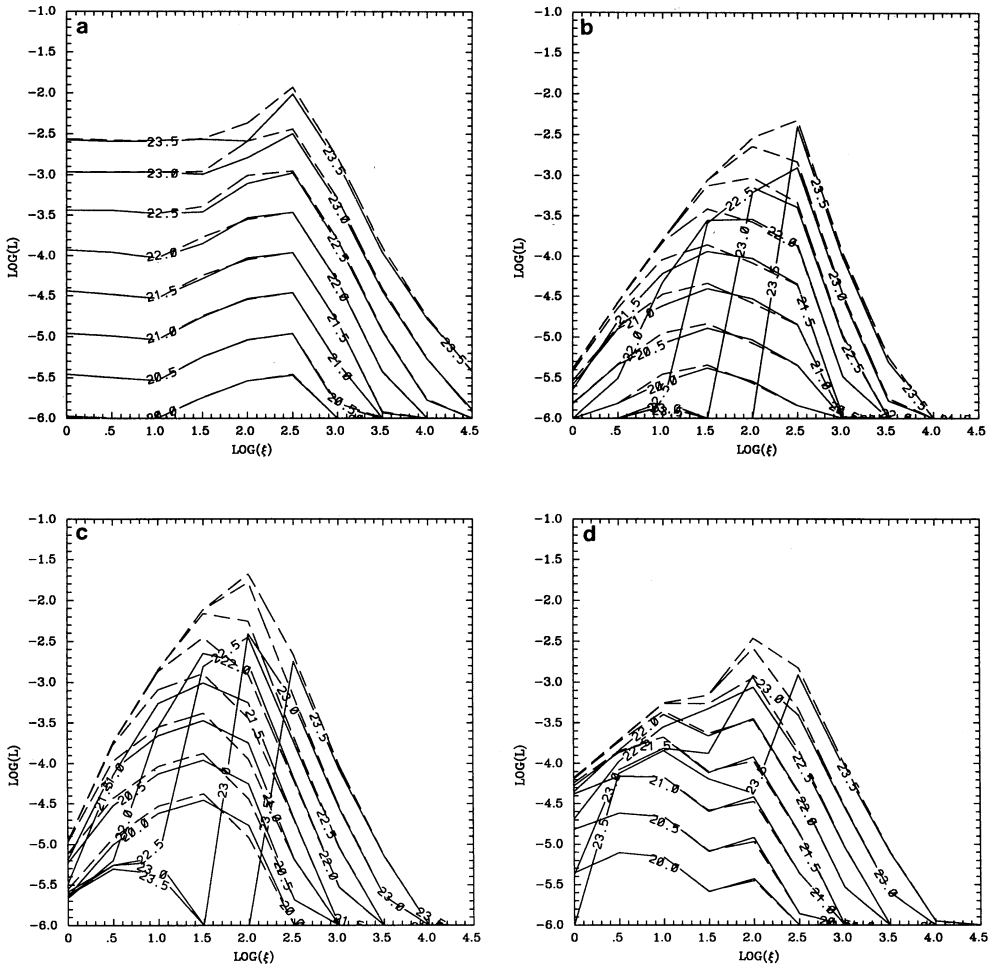

FIG. 4.—Luminosities of various emission lines emitted by constant density slabs of varying column density. Lines reflected from the illuminated face of the slab are shown as the dashed curves, and lines emitted from the unilluminated face of the slabs are shown as solid curves. Curves are labeled by the log of the slab column density (reflected curves are not labeled for clarity). The luminosity is fractional relative to the total ionizing luminosity, and the continuum is assumed to be a power law with index −0.7. The various panels are for various lines: (*a*) iron K lines; (*b*) iron L lines; (*c*) oxygen K lines; (*d*) silicon K lines.

large ξ, this quantity approaches 1.29 keV, corresponding to the energy of the Hα analog line of Fe XXVI. At small ξ, the mean energy approaches 750 eV, the energy of the L lines of Fe III, VI, IX, and X. In the intermediate region, where the L luminosity peaks, the mean energy is 0.8–1 keV.

2.3. *Effects of Spectral Shape*

All of the results discussed so far have been calculated using a power-law spectrum with energy index −1. Since line emission depends on the reprocessing of continuum photons at energies above the line, the efficiencies of line emission (relative to total luminosity) and the relative efficiencies of K and L emission depend on the shape of the spectrum. The sense of the dependence is straightforward to predict: harder spectra in the 1–10 keV band will produce more K line photons relative to L lines, and conversely softer spectra will produce a greater L/K ratio.

These results are presented in Figures 4–9. These correspond to Figures 1–3 for ionizing spectra with power-law indices −0.7 (Figs. 3–5) and −1.5 (Figs. 7–9). Again, the first figure of each set shows the emission efficiency for various lines, the second shows the mean energy, and the third shows the L/K ratio. We see that the qualitative behavior of the emission efficiency is the same for the various spectra. The scale of the efficiencies differs according to spectral hardness, according to the expectations. For the spectra we have considered the maximum L/K ratio comes from the index −1.5 power law, which can produce L/K $\simeq$ 3 at intermediate ionization parameter at high column, $N = 10^{23.5}$ cm^{-2}, where the K line equivalent width is high.

2.4. *Oxygen and Silicon K Lines*

The peak efficiencies for producing the oxygen and silicon lines are comparable to those for iron L, and their distribution in ionization parameter mimics that of the L lines. The peak of the silicon K efficiency occurs at slightly greater ionization parameter, and that of oxygen K slightly lower, although the distributions are broad enough to significantly overlap for all the ionizing spectra. This implies that these lines should appear together in the spectra of photoionized objects.

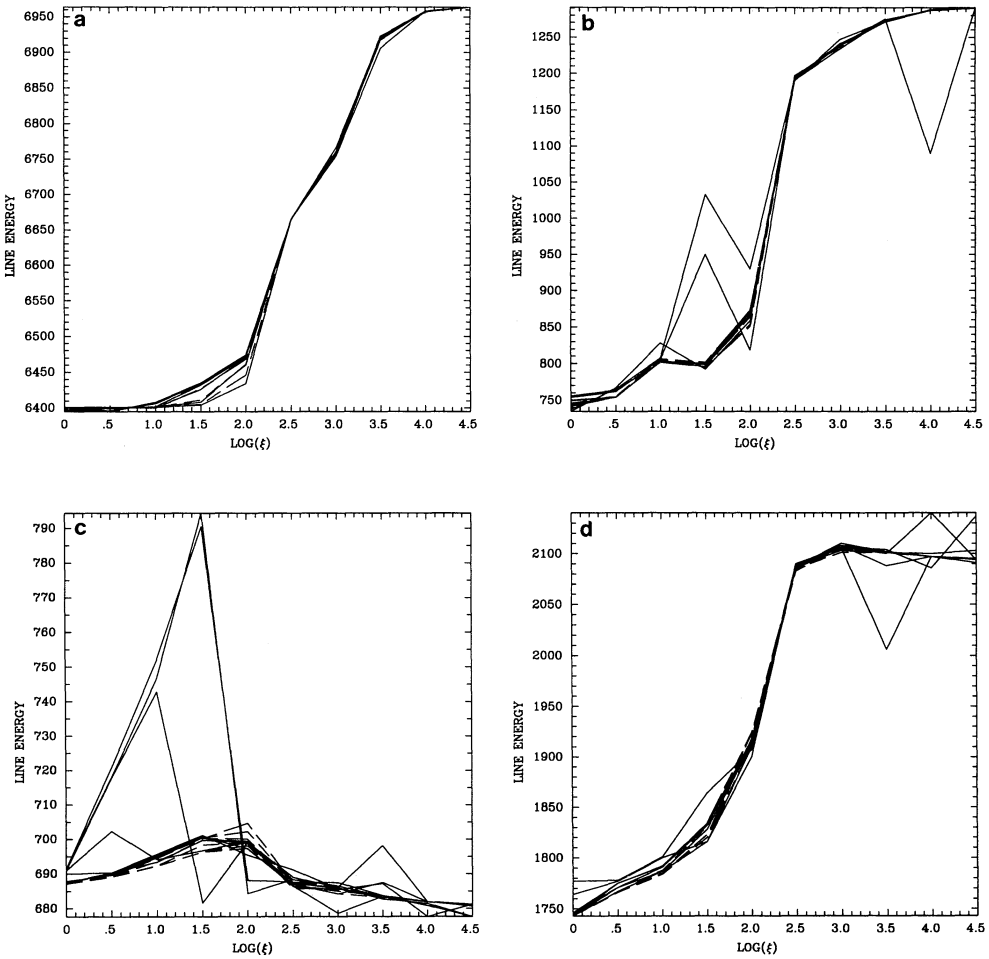

FIG. 5.—Mean energies (eV) of various emission lines emitted by constant density slabs of varying column density. Lines reflected from the illuminated face of the slab are shown as the dashed curves, and lines emitted from the unilluminated face of the slabs are shown as solid curves. The continuum is assumed to be a power law with index −0.7. The various panels are for various lines: (*a*) iron K lines; (*b*) iron L lines; (*c*) oxygen K lines; (*d*) silicon K lines.

3. DISCUSSION

We can now apply the result of the idealized models to what is known about the reprocessing environments in what are arguably the best studied objects where we expect photoionization to be important, X-ray binaries. We first discuss highly simplified models for the various emission sites in these objects and then consider some of the relevant observational constraints.

The various possible sites for reprocessed emission in these objects include an accretion disk and its associated X-ray–induced corona, companion star, accretion stream, and winds emanating from any of the above sites. For each of these we can estimate the range of likely ionization parameter and column density. It must also be emphasized that the model results for the line luminosity given in the previous section assumed that the reprocessor completely surrounded the continuum source, and that these results must be corrected for partial covering when comparing them with observations.

In the case of an accretion disk, the vertical column is likely to be greater than 10^{23} cm^{-2} (Shakura & Sunyaev 1973), although the exact value depends on the distance from the source of gravity, influence of X-ray heating, viscosity parameter, mass accretion rate, etc. An accretion disk corona (e.g., White & Holt 1982; Begelman, McKee, & Shields 1983; Begelman & McKee 1983) will have a large ionization parameter ($\log \xi \geq 4$) and can have a column up to 10^{24} cm^{-2} (e.g., Kallman & White 1988). If so, the disk/corona combination must always emit a high-energy iron line with relatively low efficiency, and a very low L/K ratio. Iron L lines require the corona to have low column density (less than 10^{23} cm^{-2}) and low ionization parameter ($\log \xi \leq 2$). The division between these two regions occurs near radii of 10^8 cm for conditions likely to occur in low-mass X-ray binaries. Large L/K ratios can be obtained only near this radius.

The observations of both L and K lines from LMXBs are subject to uncertainties owing to variability and to line blending. The situation is improving rapidly owing to advances in detectors and the launch of new instruments, so any summary of the situation is at best temporary and oversimplified. The object with the best observational data is Cyg X-2; Smale et al. (1993) have found an iron K line with energy $6.6^{+0.23}_{-0.20}$ keV and

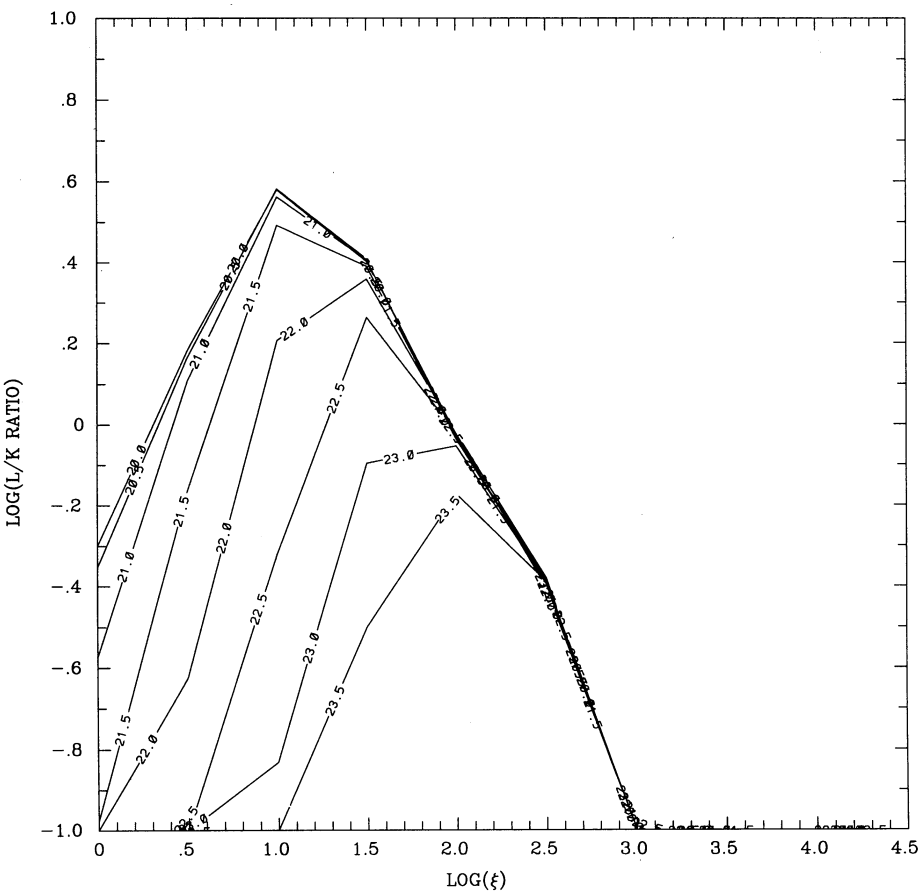

FIG. 6.—Ratio of the luminosities in the iron L and K lines as a function of ionization parameter from the results of model slabs seen in reflection shown in Fig. 3. Curves are labeled by the log of the column density.

equivalent width 60 ± 27 eV, and an L line with energy 0.99 ± 0.04 keV and equivalent width of ≥8 eV. More recent observations have refined the possible L line feature equivalent width to 30–40 eV and demonstrate variability of the feature (Smale 1995). The ratio of the fluxes in the two lines is thus in the range 0.93–3.3. This is clearly not sufficiently constrained to test any of our models, although more refined measurements will be possible in the near future which will surely do so. However, we point out that the shape of the continuum averaged over the 1–10 keV band may be approximated by a power-law slope of index −0.5; this is flatter than the continuum used to produce Figures 5 and 6, and we expect that such a spectrum cannot produce an L/K ratio in excess of 1. Furthermore, the spectra of Cyg X-2 show no obvious features at the energies of the oxygen or silicon K features. As shown in the previous section there exists virtually no region of parameter space in which the iron L emission efficiency exceeds that for both of these lines. This suggests that the elemental abundance of iron relative to oxygen or silicon (or both) in Cyg X-2 exceeds that used in these simulations. The observed equivalent width of the iron K line provides an approximate measure of the covering fraction of the disk and corona relative to the continuum source, $\Omega/4\pi \simeq 0.05$–0.1, since we expect these to have relatively high column density and so to reprocess intrinsically at nearly their maximum efficiency. This is consistent with the disk-illuminating fluxes required to produce the observed UV continuum from LMXBs via reprocessing (e.g., Ko & Kallman 1994).

Such considerations demonstrate the potential utility of the results shown in Figures 1–6 as a means of diagnosing column densities, covering fractions, elemental abundances, and ionizing continuum shapes on X-ray binaries and other astrophysical objects which are photoionized. However, quantitative determinations of these quantities are best carried out by fitting directly to the data. In order to do so we will present, in a subsequent paper, a new and more accurate set of synthetic spectra for the iron L line complex. We will then carry out a detailed test of the models and perform fits of these models directly to observations. In addition, we will provide upon request machine-readable tables of the line strengths used to construct the figures in this paper. These can be combined with line strengths measured by, for example, Gaussian fits to observed X-ray spectra, in order to infer conditions in the reprocessing gas near X-ray binaries.

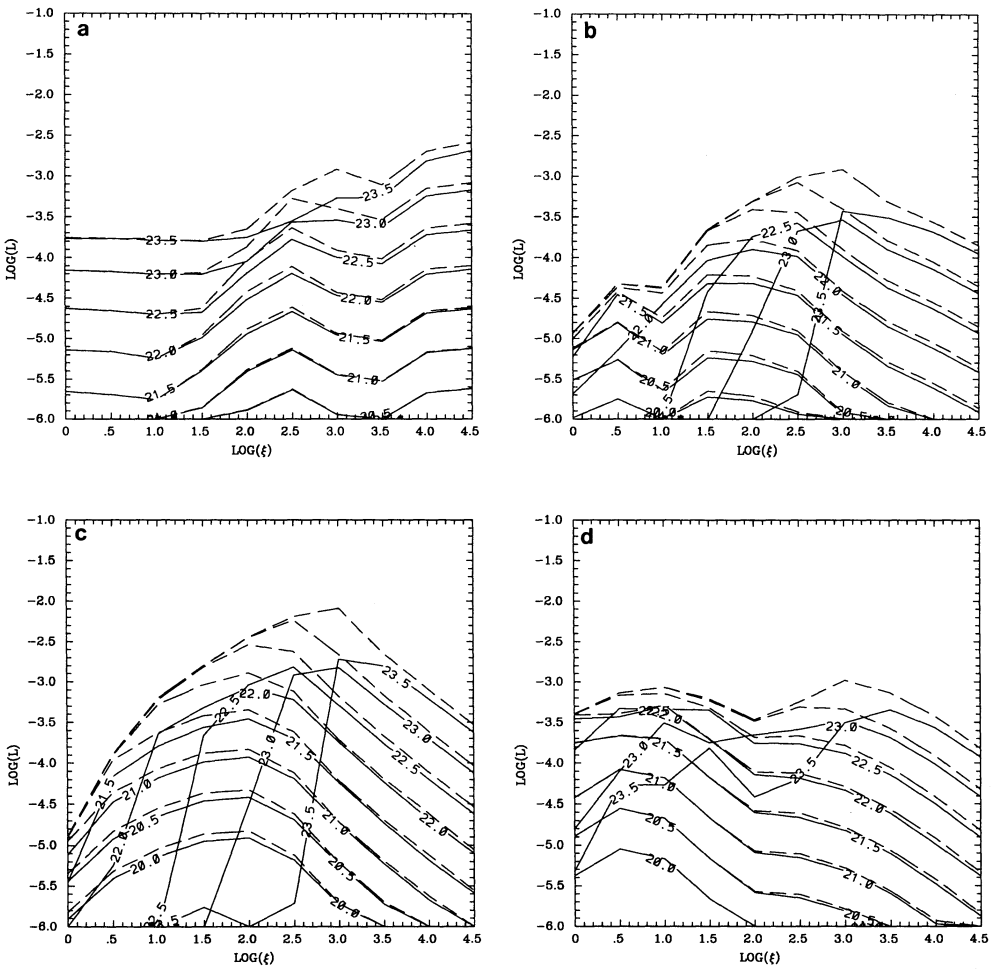

FIG. 7.—Luminosities of various emission lines emitted by constant density slabs of varying column density. Lines reflected from the illuminated face of the slab are shown as the dashed curves, and lines emitted from the unilluminated face of the slabs are shown as solid curves. Curves are labeled by the log of the slab column density (reflected curves are not labeled for clarity). The luminosity is fractional relative to the total ionizing luminosity, and the continuum is assumed to be a power law with index −1.5. The various panels are for various lines: (*a*) iron K lines; (*b*) iron L lines; (*c*) oxygen K lines; (*d*) silicon K lines.

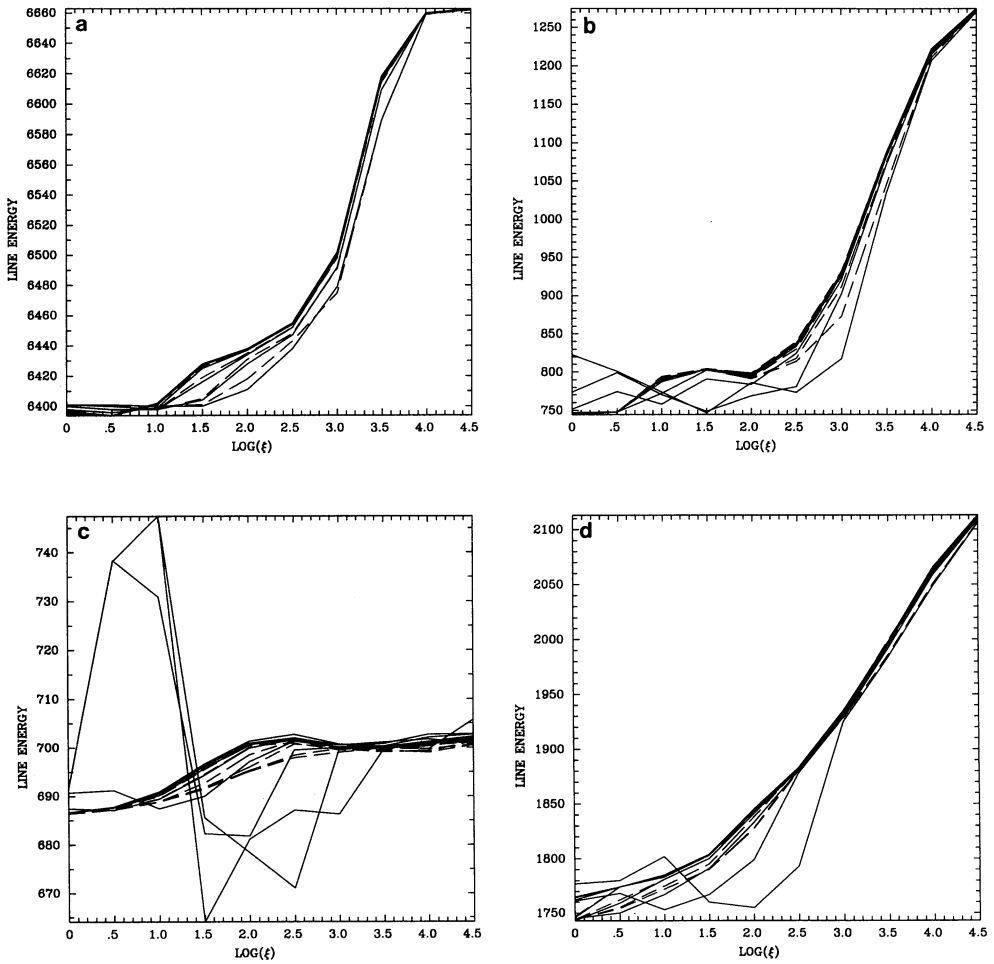

FIG. 8.—Mean energies (eV) of various emission lines emitted by constant density slabs of varying column density. Lines reflected from the illuminated face of the slab are shown as the dashed curves, and lines emitted from the unilluminated face of the slabs are shown as solid curves. The continuum is assumed to be a power law with index −1.5. The various panels are for various lines: (*a*) iron K lines; (*b*) iron L lines; (*c*) oxygen K lines; (*d*) silicon K lines.

APPENDIX A

Our models for iron line emission are calculated using the computational methods described by Kallman & McCray (1982), using the XSTAR computer code (Kallman & Krolik 1993). In this section we briefly summarize the most important points; more details may be found in the references cited above. The models consist of a plane-parallel slab of gas with continuum radiation incident from one side. The input parameters include the source spectrum, the gas composition and density, the ionization parameter at the illuminated face of the cloud (defined in § 2), and the column density of the cloud. Construction of a model consists of the simultaneous determination of the state of the gas and the radiation field as a function of distance from the illuminated face of the slab. The state of the gas at each radius follows from the assumption of a stationary local balance between heating and cooling and between ionization and recombination.

The state of the gas is defined by its temperature and by the ion abundances. All ions are predominantly in the ground state, and except for hydrogen and helium the populations of excited levels are neglected. The relative abundances of the ions of a given element are found by solving the ionization equilibrium equations under the assumption of local balance, subject to the constraint of particle number conservation for each element. Ionization balance is affected by a variety of physical processes, most notably photoionization and radiative and dielectronic recombination. The temperature is found by solving the equation of thermal equilibrium, by equating the net heating of the gas due to absorption of incident radiation with cooling due to emission by the gas. These rates are derived from integrals over the absorbed and emitted radiation spectra. Although Compton scattering is not explicitly included as a source or sink of radiation, its effect is included in the calculation of thermal balance.

The emitted spectrum includes continuum emission by bremsstrahlung and recombination and line emission by a variety of processes including recombination, collisions, and fluorescence following inner shell photoionization. Line transfer is treated using an escape probability formalism and including the effects of line destruction by collisions and continuum absorption. Transfer of the continuum is calculated using a single-stream approximation, as described in Kallman & McCray (1982).

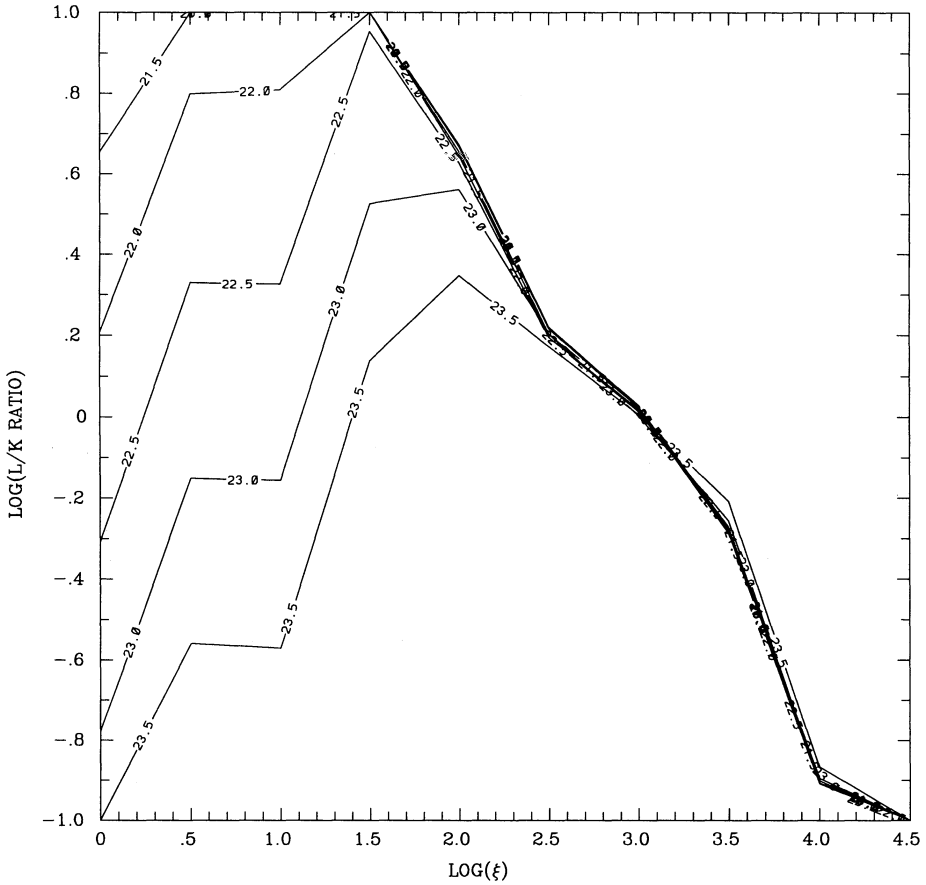

FIG. 9.—Ratio of the luminosities in the iron L and K lines as a function of ionization parameter from the results of model slabs seen in reflection shown in Fig. 7. Curves are labeled by the log of the column density.

Rates for atomic processes involving electron collisions have been modified since the publication of Kallman & McCray (1982) in order to be consistent with those used by Raymond & Smith (1977). In calculating the iron L line intensities we employ the rate data of Raymond & Smith (1977) for collisional excitation and the data of Kallman & McCray (1982) for recombination (see Kallman, Vrtilek, & Kahn 1988 for a fuller description of the calculation). We have also incorporated the L shell fluorescence yields of Jacobs & Rosznyai (1988). Recombination and ionization rates for iron have been updated to those of Arnaud & Raymond (1992). The elements Mg, Ar, Ca, and Ni have also been added. The models have a total of 168 ions, producing 1715 lines, of which 665 have energies greater than 120 eV (10 Å), and approximately 800 are resonance lines. For each ion we also calculate the emission from radiative recombination onto all the excited levels which produce resonance lines. The number of such continua is equal to the number of resonance lines in the calculation.

REFERENCES

Arnaud, M., & Raymond, J. 1992, ApJ, 398, 394
Bambynek, W., Crasemann, B., Fink, R. W., Freund, H.-U., Mark, H., Swift, C. D., Price, R. E., & Rao, P. V. 1972, Rev. Mod. Phys., 44, 716
Band, D., Klein, R., Castor, J., & Nash, J. 1990, ApJ, 362, 90
Begelman, M., & deKool, M. 1990, in Variability of Active Galactic Nuclei, ed. R. Miller & P. Wiita (Cambridge: Cambridge Univ. Press), 198
Begelman, M. C., & McKee, C. F. 1983, ApJ, 271, 89
Begelman, M. C., McKee, C. F., & Shields, G. A. 1983, ApJ, 271, 70
Jacobs, V., & Rosznyai, B. F. 1986, Phys. Rev. A., 34, 216
Kallman, T. R., & Krolik, J. H. 1993, preprint
Kallman, T. R., & McCray, R. A. 1982, ApJS, 50, 263
Kallman, T. R., Vrtilek, S. D., & Kahn, S. M. 1988, ApJ, 345, 498
Kallman, T., & White, N. E. 1988, ApJ, 341, 955
Ko, Y., & Kallman, T. R. 1994, ApJ, 431, 273
Krolik, J. H., & Kallman, T. R. 1987, ApJ, 320, L5
Liedahl, D., Kahn, S. M., Goldstein, W., & Osterheld, A. 1990, ApJ, 350, L37
Makashima, K. 1986, in The Physics of Accretion onto Compact Objects, ed. K. O. Mason, M. G. Watson, & N. E. White (Berlin: Springer), 249
Osterbrock, D. E. 1974, Astrophysics of Gaseous Nebulae (San Francisco: W. H. Freeman and Co.)
Raymond J. C., & Smith, B. H. 1977, ApJS, 35, 419
Shakura, N. I., & Sunyaev, R. A. 1973, A&A, 24, 337
Smale, A. 1995, preprint
Smale, A. P., et al. 1993, ApJ, 410, 796
Tarter, C. D., Tucker, W., & Salpeter, E. E. 1967, ApJ, 156, 943
White, N. E., & Holt, S. S. 1982, ApJ, 257, 318
White, N. E., Peacock, A., & Taylor, B. G. 1985, ApJ, 296, 475
Withbroe, G. 1971, in The Menzel Symposium on Solar Physics, Atomic Spectra, and Gaseous Nebulae, ed. K. B. Gebbie (NBS Spec. Pub. 353), 127